Polygonal patterns of confined light

EVGENY SEDOV[1,2,3,*], IRINA SEDOVA[3], SERGEY ARAKELIAN[3], AND ALEXEY KAVOKIN[1,2,4,5]

[1] School of Science, Westlake University, 18 Shilongshan Road, Hangzhou 310024, Zhejiang Province, People's Republic of China
[2] Institute of Natural Sciences, Westlake Institute for Advanced Study, 18 Shilongshan Road, Hangzhou 310024, Zhejiang Province, People's Republic of China
[3] Vladimir State University named after A. G. and N. G. Stoletovs, Gorky str. 87, Vladimir 600000, Russia
[4] School of Physics and Astronomy, University of Southampton, Southampton SO17 1NJ, United Kingdom
[5] Spin Optics Laboratory, St-Petersburg State University,1 Unlianovskaya, St-Petersburg 198504, Russia
[*] evgeny_sedov@mail.ru

Compiled March 5, 2021

We propose a technique for the generation of polygonal optical patterns in real space using a combined effect of the spin-orbit interaction and confinement of light in the plane of a dielectric optical microcavity. The spin-orbit interaction emerging from the splitting in TE and TM optical modes of the microcavity gives rise to oscillations in space of propagating macroscopic wave packets of polarized photons. Confined in a harmonic potential, the latter follow closed trajectories of a polygonal form. We demonstrate the possibility of excitation by a continuous wave resonant optical pumping of polygonal optical patterns with a controllable (both even and odd) number of vertices.

http://dx.doi.org/10.1364/ao.XX.XXXXXX

The ability of the external (orbital) degree of freedom of an electromagnetic wave influence on the internal degree of freedom which is polarization or spin is in the basis of the spin-orbit interaction (SOI) of light [1]. This influence is reciprocal. Among the mechanisms linking the orbital and spin properties of light are optical anisotropy and inhomogeneity of optical structures [2, 3], nonlinearity [4], coupling with spin non-degenerate excitations of medium [5], surface and interface effects [6]. The spin-orbit interaction is manifested in the polarization-dependent shaping of light.

The SOI induced effects become more pronounced when light is confined in a multi-interface structure which is a microcavity formed by a dielectric layer of thickness of the order of the light wavelength surrounded by a pair of distributed Bragg reflectors. The latter acting as optical filters bring the problem of characterizing an electromagnetic field to describing two optical modes of orthogonal transverse electric (TE) and transverse magnetic (TM) polarizations [7, 8]. The confinement of light in the cavity layer reduces the consideration to two spatial dimensions, $\mathbf{r} = (x, y)$. The TE and TM modes are non-degenerate, and they exhibit a strong energy splitting which acts as a source of SOI interaction of light in such system. Within the pseudospin formalism [9], the TE-TM splitting is treated as a depending of the wave vector $\mathbf{k} = (k_x, k_y)$ effective magnetic field $\mathbf{\Omega} = [\Delta(k_x^2 - k_y^2), 2\Delta k_x k_y, 0]$ of frequency $\Omega = |\mathbf{\Omega}|$ which causes precession of the Stokes (pseudospin) vector $\mathbf{S} = (S_x, S_y, S_z)$ characterizing polarization of light. The SOI Hamiltonian takes the form $H_{\mathrm{SOI}} = \hbar\mathbf{\Omega} \cdot \mathbf{S}$. The parameter Δ is the splitting constant.

In two-dimensional microcavity structures SOI it is usually treated as a tool for controlling spin degree of freedom of light including spin currents and polarization spreading over macroscopic distances [10–14]. The regime of strong coupling of light with a resonant medium is considered in such studies as a rule. Herewith the orbital behavior usually remains undisclosed. Among the exceptions is Ref. [15] in which SOI was considered as a mechanism of generating optical vortices due to the conversion of spin to the orbital angular momentum of light. Recent papers [16–18] show that SOI lies at the origin of the effect of the zitterbewegung consisting in spin-induced oscillations of a ballistic trajectory of exciton polaritons representing microcavity photons strongly coupled to excitons, excitations in semiconductor wells embedded in the microcavity structure. The optical spin Hall effect was also demonstrated for polaritons [11, 19] manifested in formation of cartwheel polarization patterns in real space.

In this letter, we promote SOI for the role of a mechanism for the spin-controlled shaping of light. We demonstrate that due to the direct influence of the spin precession on the ballistic trajectory of photons confined in a harmonic trap in the microcavity plane, regular polarization patterns coexist with polygonal intensity patterns in real space, see Fig. 1.

Formally, the polarized electric field in the microcavity structure can be described as a spinor $[\Psi_+(\mathbf{r}), \Psi_-(\mathbf{r})]^{\mathrm{T}}$ with the circularly polarized field components $\Psi_\pm(\mathbf{r})$ being eigenfunctions of the following Hamiltonian:

$$\hat{H} = \hat{T} + \hat{V} + \hat{H}_{\mathrm{SOI}} \quad (1)$$

where $\hat{T} = (\hbar^2\hat{k}^2)/2M$ is the kinetic energy operator, M is the effective mass of photons in the microcavity plane. $\hat{V} = M\omega_{\mathrm{tr}}^2\hat{r}^2/2$ is the harmonic potential characterized by the frequency ω_{tr}. To confine photons in the microcavity plane in the possible experiment, we suggest using so called mesas, which represent a local variation in the radial direction of the cavity layer thickness [20]. Another option is using concave Bragg mirrors [21]. $\hat{H}_{\mathrm{SOI}}$ is the SOI Hamiltonian written in the operator form, $\mathbf{k} \to \hat{\mathbf{k}}$, $\mathbf{S} \to \hat{\mathbf{S}}$.

In the absence of SOI, the electric field obeys the properties of a quantum harmonic oscillator, and photons resonantly injected into the structure with a wave vector obeying the equation

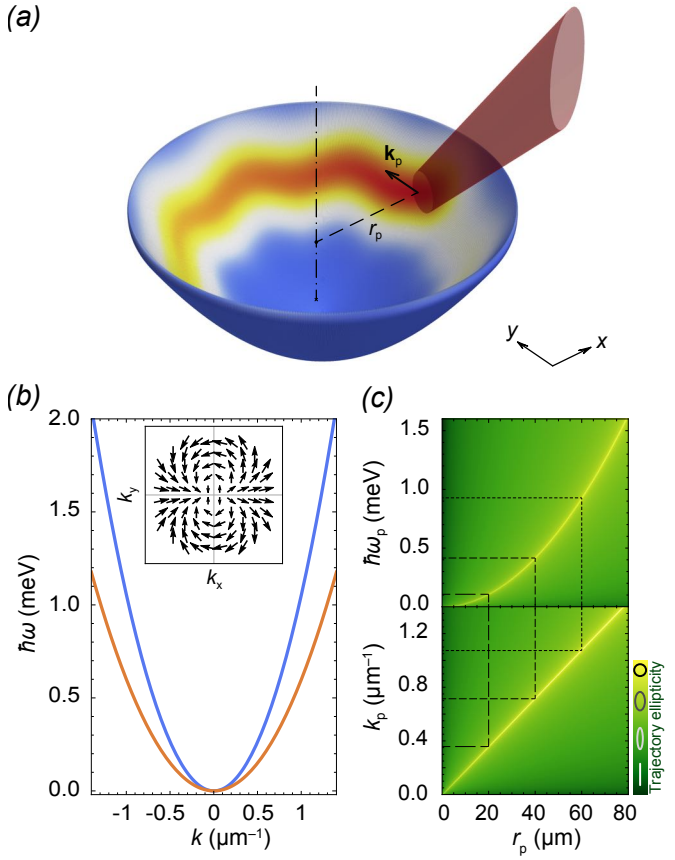

Fig. 1. (a) Schematic of excitation of polygonal patterns of photons. The CW resonant optical pump beam (red cone) of energy $\hbar\omega_p$ injects photons with the wave vector $\mathbf{k}_p$ to the structure at a distance r_p from the centre of the trap. (b) Schematic dispersion of two split TE and TM optical modes in the structure. The insert shows the effective magnetic field $\mathbf{\Omega}(\mathbf{k})$ driven by the TE-TM splitting of optical modes. (c) Illustration to the choice of the position r_p, quasimomentum k_p and energy $\hbar\omega_p$ of the pump. We take the pump resonant to the lower (TE) optical mode such that the photons injected to the structure follow trajectories close to circular (yellow area).

$T(k) = V(r)$ follow a circular trajectory keeping their polarization. In the presence of the TE-TM splitting, the structure supports two non-degenerate in energy optical modes of the corresponding polarizations, see Fig. 1b. The originated from the TE-TM splitting effective magnetic field $\mathbf{\Omega}$ (schematically shown in the insert to Fig. 1b) causes precession of the Stokes vector of propagating light according to the equation $d_t\hat{\mathbf{S}} = \hat{\mathbf{\Omega}} \times \hat{\mathbf{S}}$ which induces oscillations between the polarization dispersion branches with frequency Ω. As a result, due to the local spin-to-orbital conversion the position of propagating photons experiences oscillations with the same frequency as well. The oscillating term appears in the equation for the position operators of a propagating photon:

$$d_t\hat{r}_j = i\hbar^{-1}[\hat{T} + \hat{V}, \hat{r}_j] + i\hbar^{-1}[\hat{H}_{SOI}, \hat{r}_j], \qquad (2)$$

where $\hat{r}_j = \hat{x}, \hat{y}$. We could hide the origin of such behavior of photons behind the trendy research direction of visualization of the quantum geometric tensor and measuring the Berry curvature [5, 22]. However, such behavior can be treated in a much simple way as the zitterbewegung of light [16] on a closed path.

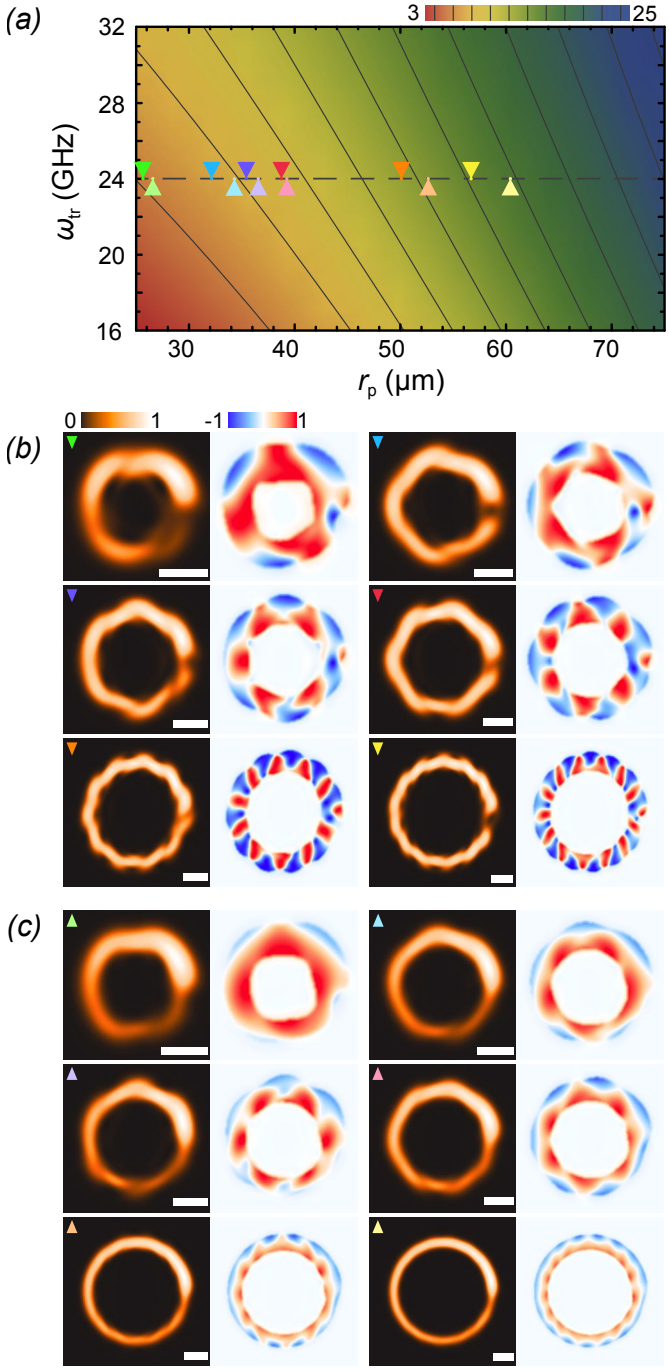

Fig. 2. (a) Schematic of the number of periods of oscillations of the center-of-mass trajectory of the optical field in one turn around the trap as a function of the position of the pump r_p and the frequency of the confining potential ω_{tr}. (b), (c) Spatial distribution of the intensity (left panels) and the degree of circular polarization (right panels) of the optical fields in the steady state. The color triangle markers in (a) indicate values of the parameters used for (b) and (c). The size bars in left panels in (b) and (c) correspond to 25 μm. The dashed horizontal line in (a) indicates $\omega_{tr} = 24$ GHz used in further simulations.

To find out the mutual effect of SOI and a harmonic trap on behavior of confined light in a possible experiment, we solve the generalized Pauli equation for the electric field spinor $|\Psi\rangle =$

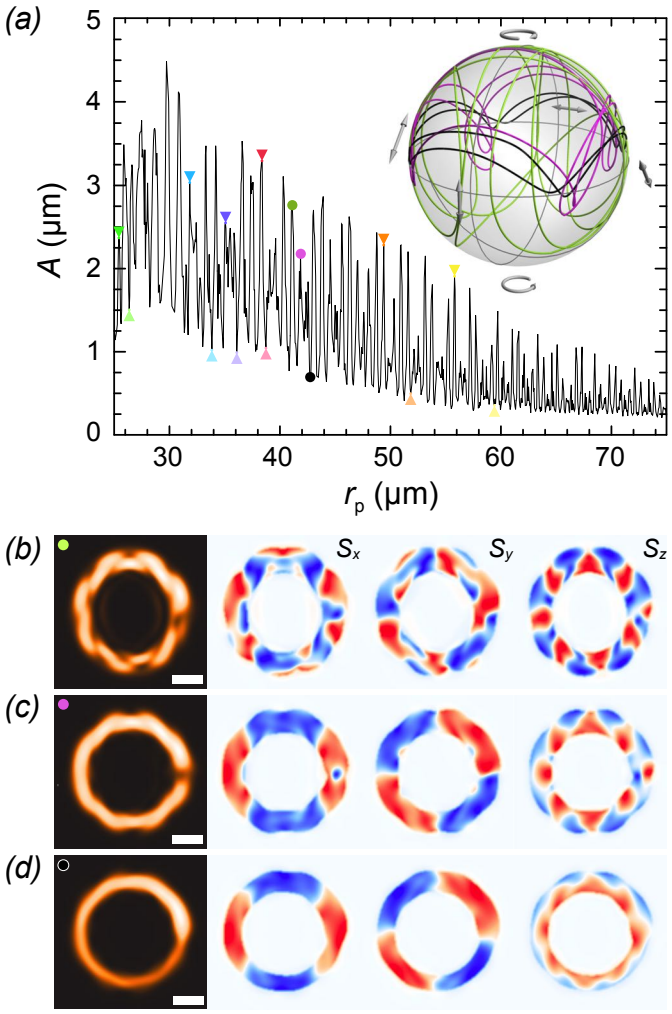

Fig. 3. (a) The dependence of the amplitude of oscillations of the center-of-mass trajectory A on the position of pump beam r_p. The insert shows trajectories on the Poincaré sphere of the Stokes vector characterizing variation of polarization of the optical field along the center-of-mass trajectory around the trap. (b)–(d) Spatial distribution of the intensity and the polarizations components of the optical fields in the form close to the octagonal in the steady state. The color circular markers in (a) indicate values of the parameters used for (b)–(d). The color triangle markers in (a) indicate values of the parameters used for (b) and (c) in Fig. 2. The colors of lines in the insert in (a) match the colors of markers on the corresponding panels (b)–(d).

$[\Psi_+(t,\mathbf{r}),\Psi_-(t,\mathbf{r})]^{\mathrm{T}}$ in the basis of circular polarizations [15]:

$$i\partial_t|\Psi\rangle = \left[\hbar^{-1}\hat{H} - (\omega_p + i\gamma)\right]|\Psi\rangle + |F\rangle. \quad (3)$$

γ is the photon decay rate. The last term in Eq. (3) given as $|F\rangle = F(\mathbf{r})|f\rangle$ describes pumping of photons in the microcavity. Light is injected into the structure by the CW optical pump beam of a Gaussian shape

$$F(\mathbf{r}) \propto exp[-(\mathbf{r}-\mathbf{r}_p)^2/2w^2]exp[i\mathbf{k}_p\mathbf{r}] \quad (4)$$

shifted by $\mathbf{r}_p = (r_p, 0)$ from the center of the harmonic trap. The width of the pump beam is $w = \sqrt{\hbar/M\omega_{tr}}$. The pump is taken resonant to the lower (TE) photonic dispersion branch with the central wave vector $\mathbf{k}_p = (0, k_p)$ and the energy $\hbar\omega_p$ chosen such that the center-of-mass trajectory of the photonic wave packet was close to circular. Namely, we link the model parameters r_p, k_p and ω_p by the following equation: $\hbar\omega_p/2 = \hbar^2k_p^2/2M_{TE} = V(r_p)$, where $M_{TE} = \hbar M/(\hbar - \Delta M)$ is the effective mass of photons of the TE branch. Illustration to the choice of the model parameters is given in Fig. 1c. The vector $|f\rangle = (f_+, f_-)^{\mathrm{T}}$ is responsible for the polarization of the pump; $\langle f|f\rangle = 1$. We take the following values of the parameters for modelling. The effective photon mass in the cavity plane is $M = 7\times10^{-5}m_e$, where m_e is the free electron mass. The TE-TM splitting constant is $\hbar\Delta = 300\,\mu$eV μm^2. Photons in optical microcavities possess a finite lifetime which is determined by the Q-factor of the microcavity. In our simulations, we used the photon lifetime of $\gamma^{-1} = 150$ ps which is a realistic estimate at present. Recent achievements in developing photonic microstructures [23, 24] have made it routine to grow structures that provide photon lifetimes of many hundreds of picoseconds which allows photons to travel by the distance of millimetres from the injection spot. The harmonic trap frequency is taken as $\omega_{tr} = 24$ GHz unless otherwise specified. The polarization of the pump beam is taken right-circular, $|f\rangle = (1,0)^{\mathrm{T}}$.

In our numerical experiments, we track the center-of-mass trajectory of photonic wave packets in the steady state. The color map in Fig. 2a shows a number of periods n of oscillations of the trajectory on one turn around the harmonic trap as a function of the position of the pump beam r_p and the frequency of the harmonic trap ω_{tr}. A rounded number of the periods determines the number of sides of the emerging polygon patterns. For a classical spinning particle following the trajectory described by Eq. (2) where operators are replaced with their expectation values, n can be estimated as $n = \Delta M k_p r_p/\hbar^2$. In the possible experiment, the photonic wave packet is the closest to the classical condition at high energies and, as a consequence, at large distances r_p from the center of the harmonic trap [25]. The dependence undergoes distortions for the wave packet of finite width when the latter is comparable with the period of oscillations.

Figures 2b–2c show examples of polygonal light intensity patterns accompanied by the cogwheel-shape patterns of the circular polarization degree. The emerging patterns can be divided into two types. For the first type (Fig. 2b) vertices are more significantly pronounced that for the second type (Fig. 2c). This peculiarity has a simple explanation. A long lifetime of photons in the structure allows the photon wave packet to propagate over distances exceeding length of its closed trajectory in the trap. This leads to self-interference of light when just injected photons interfere with ones after one and subsequent turns around the trap. The phase shift between different parts of the self-interfering photon field varies depending on the displacement r_p which leads to either strengthening or weakening the effect due to the constructive or destructive interference. For both types of patterns, the circular polarization degree experiences oscillations around the trap. Nevertheless, for the patterns of the second type a clear separation of the left-circularly (blue) and right-circularly (red) polarized components of the electric field in the radial direction is observed. One of the manifestations of the self-interference is the presence of a slit in the intensity distribution near the pump spot for the intensity patterns of the first type. Our simulations (not presented in the letter) show that when the photon lifetime is small enough to

suppress the self-interference, only one type of patterns exists characterized by pronounced vertices and the intensity rapidly decreasing with azimuth angle. The considerable increase in the photon lifetime makes the self-interference effects dominating and leads to formation of intensity and polarization patterns of intricate structure.

In Fig. 3a we show the variation of the amplitude A of oscillations of the center-of-mass trajectory with the pump position r_p in a trap with the fixed frequency ω_tr. The dependence $A(r_\mathrm{p})$ is strongly non-monotonic. The average amplitude decreases with the increasing distance r_p and, consequently, the increasing wave number k_p of the pump beam, which is in line with the interpretation of the observed effect as the zitterbewegung of light [16]. The dependence $A(r_\mathrm{p})$ is more complicated at small r_p when the period of oscillations is comparable with the length of the trajectory and the width of the photonic wave packet. In Fig. 3a we indicate the parameters used for modelling the polygon patterns in Fig. 2b–2c. It is clearly seen that the local maxima of the amplitude correspond to the patterns with the pronounced vertices and a slit in the intensity distribution. Herewith the amplitude of the unbroken patterns corresponds to the local minima of the dependence $A(r_\mathrm{p})$. The system is very sensitive to the shift of the pump beam due to the discussed earlier self-interference effect. In panels 3b–3d we show the octagonal intensity patterns accompanied by the polarization patterns for the linear (S_x), diagonal/antidiagonal (S_y) and circular (S_z) components. Clear linear polarization domains are observed for the electric field with the smooth intensity distribution (panels 3c and 3d). The linear polarization plane rotates twice around the harmonic trap following the direction of the effective field $\mathbf{\Omega}$. The trajectories of the Stokes vector of such states are located near the equator of the Poincaré sphere, see insert in Fig. 3a. The spatial separation in linear polarizations allows considering our system as a polarization rectifier of cw light, analogously to one for optical pulses suggested in [25].

In this letter, we have proposed an approach to creating optical patterns of new geometry using the effect of polarization of light on its orbital behavior. An alternative approach to creating polygon patterns in optical microcavities was discussed in [26]. It exploits the parametric instability in a nonlinear system under the strong coupling of light with excitons in embedded quantum wells. Photonic molecular states of polygonal shape have been reported recently in [27], where shaping of light intensity was achieved in the regime of condensation of exciton-polaritons in a set of micropillars arranged in the form of a hexagon. An important peculiarity of our approach is that the light polygons can be formed in a linear regime for pure photonic modes. Herewith, our approach can be effectively extended to the case of the strong light-matter coupling for observing polygonal patterns of exciton polaritons in optically induced traps [25, 28].

Funding. Westlake University (041020100118); Leading Innovative and Entrepreneur Team Introduction Program of Zhejiang (2018R01002); Council for Grants of the President of the Russian Federation (MK-4729.2021.1.2); the Russian Foundation for Basic Research (21-52-10005); Saint Petersburg State University (28874264); the Royal Society (IEC\R2\202148).

Disclosures. The authors declare no conflicts of interest.

Data availability. Data underlying the results presented in this paper are not publicly available at this time but may be obtained from the authors upon reasonable request.

REFERENCES

1. K. Y. Bliokh, F. J. Rodríguez-Fortuño, F. Nori, and A. V. Zayats, Nat. Photonics **9**, 796 (2015).
2. L. Marrucci, C. Manzo, and D. Paparo, Phys. Rev. Lett. **96**, 163905 (2006).
3. J. Lin, J. P. B. Mueller, Q. Wang, G. Yuan, N. Antoniou, X.-C. Yuan, and F. Capasso, Science **340**, 331 (2013).
4. M. E. Ketara and E. Brasselet, Opt. Lett. **37**, 602 (2012).
5. A. Gianfrate, O. Bleu, L. Dominici, V. Ardizzone, M. De Giorgi, D. Ballarini, G. Lerario, K. W. West, L. N. Pfeiffer, D. D. Solnyshkov, D. Sanvitto, and G. Malpuech, Nature **578**, 381 (2020).
6. K. Y. Bliokh and Y. P. Bliokh, Phys. Rev. Lett. **96**, 073903 (2006).
7. G. Panzarini, L. C. Andreani, A. Armitage, D. Baxter, M. S. Skolnick, V. N. Astratov, J. S. Roberts, A. V. Kavokin, M. R. Vladimirova, and M. A. Kaliteevski, Phys. Rev. B **59**, 5082 (1999).
8. A. Kavokin, J. Baumberg, G. Malpuech, and F. Laussy, *Microcavities*, Series on Semiconductor Science and Technology (OUP Oxford, 20017), 2nd ed.
9. K. V. Kavokin, I. A. Shelykh, A. V. Kavokin, G. Malpuech, and P. Bigenwald, Phys. Rev. Lett. **92**, 017401 (2004).
10. E. S. Sedov and A. V. Kavokin, Sci. Reports **7**, 9797 (2017).
11. A. Kavokin, G. Malpuech, and M. Glazov, Phys. Rev. Lett. **95**, 136601 (2005).
12. D. Schmidt, B. Berger, M. Bayer, C. Schneider, M. Kamp, S. Höfling, E. Sedov, A. Kavokin, and M. Aßmann, Phys. Rev. B **96**, 075309 (2017).
13. D. Caputo, E. S. Sedov, D. Ballarini, M. M. Glazov, A. V. Kavokin, and D. Sanvitto, Commun. Phys. **2**, 165 (2019).
14. M. Sich, L. E. Tapia-Rodriguez, H. Sigurdsson, P. M. Walker, E. Clarke, I. A. Shelykh, B. Royall, E. S. Sedov, A. V. Kavokin, D. V. Skryabin, M. S. Skolnick, and D. N. Krizhanovskii, ACS Photonics **5**, 5095 (2018).
15. F. Manni, K. G. Lagoudakis, T. K. Paraïso, R. Cerna, Y. Léger, T. C. H. Liew, I. A. Shelykh, A. V. Kavokin, F. Morier-Genoud, and B. Deveaud-Plédran, Phys. Rev. B **83**, 241307 (2011).
16. E. S. Sedov, Y. G. Rubo, and A. V. Kavokin, Phys. Rev. B **97**, 245312 (2018).
17. E. S. Sedov, I. E. Sedova, S. M. Arakelian, and A. V. Kavokin, New J. Phys. **22**, 083059 (2020).
18. I. E. Sedova, E. S. Sedov, S. M. Arakelian, and A. V. Kavokin, Bull. Russ. Acad. Sci. Phys. **84**, 1453 (2020).
19. E. Kammann, T. C. H. Liew, H. Ohadi, P. Cilibrizzi, P. Tsotsis, Z. Hatzopoulos, P. G. Savvidis, A. V. Kavokin, and P. G. Lagoudakis, Phys. Rev. Lett. **109**, 036404 (2012).
20. R. I. Kaitouni, O. El Daïf, A. Baas, M. Richard, T. Paraiso, P. Lugan, T. Guillet, F. Morier-Genoud, J. D. Ganière, J. L. Staehli, V. Savona, and B. Deveaud, Phys. Rev. B **74**, 155311 (2006).
21. S. Dufferwiel, F. Li, E. Cancellieri, L. Giriunas, A. A. P. Trichet, D. M. Whittaker, P. M. Walker, F. Fras, E. Clarke, J. M. Smith, M. S. Skolnick, and D. N. Krizhanovskii, Phys. Rev. Lett. **115**, 246401 (2015).
22. O. Bleu, G. Malpuech, Y. Gao, and D. D. Solnyshkov, Phys. Rev. Lett. **121**, 020401 (2018).
23. B. Nelsen, G. Liu, M. Steger, D. W. Snoke, R. Balili, K. West, and L. Pfeiffer, Phys. Rev. X **3**, 041015 (2013).
24. D. M. Myers, B. Ozden, M. Steger, E. Sedov, A. Kavokin, K. West, L. N. Pfeiffer, and D. W. Snoke, Phys. Rev. B **98**, 045301 (2018).
25. E. S. Sedov, Y. G. Rubo, and A. V. Kavokin, Light. Sci. & Appl. **8**, 79 (2019).
26. C. E. Whittaker, B. Dzurnak, O. A. Egorov, G. Buonaiuto, P. M. Walker, E. Cancellieri, D. M. Whittaker, E. Clarke, S. S. Gavrilov, M. S. Skolnick, and D. N. Krizhanovskii, Phys. Rev. X **7**, 031033 (2017).
27. V. G. Sala, D. D. Solnyshkov, I. Carusotto, T. Jacqmin, A. Lemaître, H. Terças, A. Nalitov, M. Abbarchi, E. Galopin, I. Sagnes, J. Bloch, G. Malpuech, and A. Amo, Phys. Rev. X **5**, 011034 (2015).
28. A. Askitopoulos, A. V. Nalitov, E. S. Sedov, L. Pickup, E. D. Cherotchenko, Z. Hatzopoulos, P. G. Savvidis, A. V. Kavokin, and P. G. Lagoudakis, Phys. Rev. B **97**, 235303 (2018).